Titan's atomic hydrogen corona

P. Hedelt, Y. Ito, H.U. Keller, R. Reulke, P. Wurz, H. Lammer, H. Rauer, L. Esposito

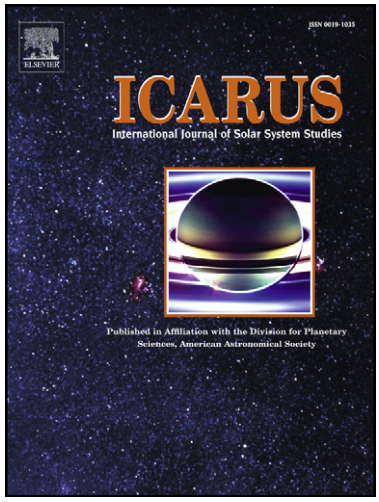

Titan's atomic hydrogen corona

P. Hedelt, Y. Ito, H.U. Keller, R. Reulke, P. Wurz, H. Lammer, H. Rauer, L. Esposito

PII: S0019-1035(10)00234-4
DOI: 10.1016/j.icarus.2010.06.012
Reference: YICAR 9464

To appear in: *Icarus*

Received Date: 13 November 2009
Revised Date: 4 June 2010
Accepted Date: 10 June 2010

Please cite this article as: Hedelt, P., Ito, Y., Keller, H.U., Reulke, R., Wurz, P., Lammer, H., Rauer, H., Esposito, L., Titan's atomic hydrogen corona, *Icarus* (2010), doi: 10.1016/j.icarus.2010.06.012

Titan's atomic hydrogen corona

P. Hedelt[*,a,b], Y. Ito[c], H.U. Keller[d], R. Reulke[e], P. Wurz[f], H. Lammer[g], H. Rauer[a,h], L. Esposito[i]

[a] *Institut für Planetenforschung, Deutsches Zentrum für Luft- und Raumfahrt, Rutherfordstr. 2, 12489 Berlin, Germany*
[b] *Laboratoire d'Astrophysique de Bordeaux, Université de Bordeaux - CNRS, 2, rue de l'Observatoire, BP 89, F-33271 Floirac cedex, France*
[c] *Japan Manned Space Systems Corporation, Tsukuba, Urban Square Tsuchiura Bldg., 1-1-26 Kawaguchi Tsuchiura-shi, Ibaraki Prefecture 300-0033, Japan*
[d] *Max-Planck-Institut für Sonnensystemforschung, Max-Planck-Str. 2, 37191 Katlenburg-Lindau Germany*
[e] *Institut für Verkehrsforschung, Deutsches Zentrum für Luft- und Raumfahrt, Rutherfordstr. 2, 12489 Berlin, Germany*
[f] *Physikalisches Institut, Universität Bern, Sidlerstrasse 5, CH-3012 Bern, Switzerland*
[g] *Space Research Institute, Austrian Academy of Sciences, Schmiedlstr. 6, A-8042 Graz, Austria*
[h] *Zentrum für Astronomie und Astrophysik, Technische Universität Berlin, Hardenbergstr. 36, 10623 Berlin, Germany*
[i] *University of Colorado, Laboratory for Atmospheric and Space Physics, 1234 Innovation Drive, Boulder, CO 80303-7814, USA*

Abstract

Based on measurements performed by the Hydrogen Deuterium Absorption Cell (HDAC) aboard the Cassini orbiter, Titan's atomic hydrogen exosphere is investigated. Data obtained during the T9 encounter are used to infer the distribution of atomic hydrogen throughout Titan's exosphere, as well as the exospheric temperature.

The measurements performed during the flyby are modeled by performing Monte Carlo radiative transfer calculations of solar Lyman-α radiation, which

[*]Corresponding author, Tel. +33 557 776 127
Email addresses: pascal.hedelt@obs.u-bordeaux1.fr (P. Hedelt), itoyuichi2000@yahoo.co.jp (Y. Ito), keller@mps.mpg.de (H.U. Keller), Ralf.Reulke@dlr.de (R. Reulke), peter.wurz@space.unibe.ch (P. Wurz), helmut.lammer@oeaw.ac.at (H. Lammer), heike.rauer@dlr.de (H. Rauer), esposito@lasp.colorado.edu (L. Esposito)

[1]Proposed running head: Titan's atomic hydrogen corona

is resonantly scattered on atomic hydrogen in Titan's exosphere. Two different atomic hydrogen distribution models are applied to determine the best fitting density profile. One model is a static model that uses the Chamberlain formalism to calculate the distribution of atomic hydrogen throughout the exosphere, whereas the second model is a particle model, which can also be applied to non-Maxwellian velocity distributions.

The density distributions provided by both models are able to fit the measurements although both models differ at the exobase: Best fitting exobase atomic hydrogen densities of $n_{\mathrm{H}} = (1.5 \pm 0.5) \cdot 10^4\,\mathrm{cm}^{-3}$ and $n_{\mathrm{H}} = (7 \pm 1) \cdot 10^4\,\mathrm{cm}^{-3}$ were found using the density distribution provided by both models, respectively. This is based on the fact that during the encounter, HDAC was sensitive to altitudes above about 3,000 km, hence well above the exobase at about 1,500 km. Above 3,000 km, both models produce densities which are comparable, when taking into account the measurement uncertainty.

The inferred exobase density using the Chamberlain profile is a factor of about 2.6 lower than the density obtained from Voyager 1 measurements and much lower than the values inferred from current photochemical models. However, when taking into account the higher solar activity during the Voyager flyby, this is consistent with the Voyager measurements. When using the density profile provided by the particle model, the best fitting exobase density is in perfect agreement with the densities inferred by current photochemical models.

Furthermore, a best fitting exospheric temperature of atomic hydrogen in the range of $T_{\mathrm{H}} = (150 - 175) \pm 25\,\mathrm{K}$ was obtained when assuming an isothermal exosphere for the calculations. The required exospheric temperature depends on the density distribution chosen. This result is within the temperature range determined by different instruments aboard Cassini. The inferred temperature is close to the critical temperature for atomic hydrogen, above which it can escape hydrodynamically after it diffused through the heavier background gas.

Key words: Titan, atmosphere, Atmospheres, structures, Ultraviolet observations, Satellites, atmospheres, Spectroscopy

1. Introduction

With a radius of 2,575 km, Titan is the biggest moon in the Saturnian system and the second biggest moon in the entire solar system. It is the only moon having a dense atmosphere, with a surface pressure of 1.5 bar (Fulchignoni et al. 2005), consisting mainly of nitrogen (N_2, 96%) and methane (CH_4, 4%). The low surface temperature of 94 K (Fulchignoni et al. 2005) and the low surface gravity of Titan (1.35 $m\,s^{-2}$) give rise to a completely different atmospheric chemistry than on Earth. The coupled chemistry between nitrogen and methane leads to high atmospheric abundances of complex nitrogen/carbon compounds, caused primarily by the breakup of methane into carbon and hydrogen compounds in the upper atmosphere, which is induced by solar ultraviolet radiation (see e.g. Strobel 1983). The low gravity of Titan allows atomic hydrogen to escape effectively from the atmosphere, resulting in a low atmospheric hydrogen abundance and hence a rich hydrocarbon production.

Titan's neutral exosphere consists mainly of N_2, CH_4, H_2 and H. The exobase densities (at an altitude of about 1,500 km) of the former three constituents have been recently measured in-situ by the Ion Neutral Mass Spectrometer (INMS, Waite et al. 2004) aboard the Cassini orbiter. The density of atomic hydrogen, however, could not be measured directly. In the past, the exobase density of atomic hydrogen has been inferred only once from measurements during the Voyager 1 flyby in 1980 (Broadfoot et al. 1981). Atomic hydrogen exobase densities inferred from current photochemical models that rely on recent data acquired by Cassini are up to a factor of two higher than the Voyager measurement (cf. Table 1).

The exospheric temperature has been determined by instruments aboard the Cassini orbiter. These measurements indicate exospheric temperatures in the range of 149 K up to 250 K. In order to understand the evolution of Titan's atmosphere, it is important to determine the exospheric temperature more precisely, since the critical temperature above which atomic hydrogen on Titan features diffusion limited hydrodynamic outflow is reached above about 178 K.

This work aims at deriving the exospheric atomic hydrogen density distribution based on data from the Hydrogen Deuterium Absorption Cell (HDAC) aboard the Cassini orbiter, which have been obtained during the Cassini T9 flyby in 2005. We furthermore concentrate on determining the exospheric temperature.

HDAC was originally designed to directly determine the D/H ratio from their respective Lyman-α emission lines. Since the deuterium absorption cell is not working properly due to contamination with atomic hydrogen, we only use data from the hydrogen cell to determine the atomic hydrogen distribution in Titan's exosphere.

This paper is structured as follows: Section 2 summarizes the latest information about Titan's exosphere and the atomic hydrogen content of the exosphere. Section 3 gives a detailed instrument description, followed by a summary of the measurements during the T9 flyby in section 4. Our radiative transfer model is described in detail in section 5. In section 6 the density models are summarized which calculate the distribution of atomic hydrogen within the radiative transfer model boundaries. Finally the fit to measured data is performed in section 7. The paper finishes with the results and conclusions in section 8.

2. Titan's exosphere

The exosphere represents the transition region from the gravitationally bound atmosphere to free interplanetary space. Within the exosphere, the mean free path of an atmospheric particle is greater than the scale height of the atmosphere, hence collisions between particles become negligible. The main neutral components of Titan's exosphere are N_2, CH_4, H_2 and H (de La Haye et al. 2007b; Cui et al. 2009; Magee et al. 2009), which has been confirmed recently by INMS measurements (see below).

The exobase is commonly defined as the altitude where the mean free path of an atmospheric particle is equal to the scale height of the atmosphere. In reality, the transition between the atmosphere and the exosphere however extends over a significant altitude region. Titan's exobase altitude has recently been determined in-situ by INMS measurements. By fitting the measured N_2 and CH_4 data, exobase altitudes between 1,400 km and 1,500 km have been determined by de La Haye et al. (2007b). For this paper, we place the exobase at 1,500 km.

Furthermore, de La Haye et al. (2007b) found temperatures below 1,500 km altitude in the range of 149 K to 158 K. Above the exobase, the authors fitted the data using the method of Chamberlain (1963) to determine exobase temperatures of 149 K to 205 K when fitting the N_2 data, whereas for CH_4 temperatures in the range of 149 K to 223 K are necessary to fit the data. Above 1,700 km de La Haye et al. (2007a) found an enhanced suprathermal

population. To account for this, they constructed another exospheric model based on the Liouville theorem. They found that an exobase energy distribution using a kappa function, which is essentially the sum of Maxwellian functions, as well as an analytical power function were able to fit the measured N_2 and CH_4 profiles. Most recently, Cui et al. (2009) determined a global temperature of 151.0±1.5 K below 1,500 km altitude based on INMS data during 15 flybys. The temperature was inferred using a simple barometric relation to fit the N_2 data. As a comparison, data obtained during the Voyager Titan encounter in 1980 yielded a thermospheric temperature in the range of 153 – 158 K (Vervack et al. 2004). The exospheric temperature has also been constrained using data from the Ultraviolet Imaging Spectrograph (UVIS, Esposito et al. 2004) to 150 K – 250 K (D. Shemansky, priv. com.). The determination of the exobase temperature is important, since atomic hydrogen in Titan's atmosphere is close to diffusion limited hydrodynamical outflow conditions (see below).

Simultaneous to fitting exospheric temperatures, de La Haye et al. (2007b) have also determined the neutral densities of N_2 and CH_4. Furthermore, Cui et al. (2008) determined the H_2 density using INMS data. Unfortunately, the density of atomic hydrogen could not be measured directly by the INMS instrument. This is because the INMS chamber walls have a certain probability to adsorb atoms and molecules entering the instrument orifice, which may further undergo complicatedchemical processes at the walls before being released with a time delay (Vuitton et al. 2008). Atomic hydrogen is very reactive, hence INMS atomic hydrogen measurements are not reliable.

There exists only one atomic hydrogen exobase density inferred from direct measurements. From Lyman-α observations of Voyager, Broadfoot et al. (1981) reported an exobase atomic hydrogen density of $4 \cdot 10^4$ cm^{-3}. However, current photochemical models that rely on latest data from the Cassini mission provide exobase densities that are higher than the measurement by a factor of up to two. Garnier et al. (2007) used an updated version of the Toublanc model (Toublanc et al. 1995) and obtained a density of $4.6 \cdot 10^4$ cm^{-3}. de La Haye et al. (2007a) have inferred the exobase density from modeling fast neutrals in the exosphere with a hot to thermal neutral atomic hydrogen ratio of $5 \cdot 10^{-5}$. They give a fast neutral exobase density of 4 cm^{-3}, from which a thermal atomic hydrogen exobase density of $8 \cdot 10^4$ cm^{-3} can be derived, which is higher than the densities published before. The fast neutral exobase density has been derived from photochemical modeling, whereas the hot to thermal neutral ratio has been inferred using a method based on

the Liouville theorem, as described in de La Haye et al. (2007b). Most recently, Krasnopolsky (2009) found an exobase density of about $7 \cdot 10^4\,\mathrm{cm}^{-3}$ from photochemical modeling. Thus, the exobase atomic hydrogen densities found in the literature range from $4 \cdot 10^4\,\mathrm{cm}^{-3}$ up to $8 \cdot 10^4\,\mathrm{cm}^{-3}$ (cf. Table 1).

Titan's atmospheric hydrogen is mainly produced by the dissociation of methane at approximately 700 km and higher (Wilson and Atreya 2004). The main pathway of the methane dissociation is given by the following reactions (Wang et al. 2000), with q being the branching ratio of each reaction:

$$\begin{aligned}
\mathrm{CH_4} + \mathrm{h}\nu &\rightarrow {}^1\mathrm{CH_2} + \mathrm{H_2} \qquad (q = 0.584)\\
\mathrm{CH_4} + \mathrm{h}\nu &\rightarrow \mathrm{CH_3} + \mathrm{H} \qquad (q = 0.291)\\
\mathrm{CH_4} + \mathrm{h}\nu &\rightarrow \mathrm{CH} + \mathrm{H_2} + \mathrm{H} \qquad (q = 0.07)\\
\mathrm{CH_4} + \mathrm{h}\nu &\rightarrow {}^1\mathrm{CH_2} + \mathrm{H} + \mathrm{H} \qquad (q = 0.055)
\end{aligned}$$

One key parameter for better understanding the origin of Titan's exosphere is the 0.024 eV/amu escape energy needed to escape from Titan's gravity (the escape velocity is $\mathrm{v_{Esc}} = 2,115$ m/s from the exobase). For a nitrogen atom, 0.34 eV are needed to gravitationally escape, for a carbon atom 0.29 eV, and for a hydrogen atom only 0.024 eV. Hydrogen has thus a large scale height in the exosphere and a significant atmospheric loss via Jeans escape.

Using INMS data, Strobel (2008, 2009) as well as Yelle et al. (2008) found strong escape rates for $\mathrm{N_2}$ and $\mathrm{CH_4}$. They required slow hydrodynamic escape of these species in order to describe the escape rates found. In their model they assumed that the upward flow below the exobase is driven by thermal conduction from below. This conduction furthermore acts above the exobase, yielding the slow hydrodynamic escape.

However, Tucker and Johnson (2009) found no evidence for slow hydrodynamic escape to act in Titan's exosphere. Using an Direct Simulation Monte Carlo (DSMC) model, they conclude that either the Strobel model is incorrect or the size of the Jeans parameter (which will be discussed later) is not sufficient to describe the deviations from Jeans escape. They found that thermal conduction did not cause any significant enhancement in their model since it does not apply above the exobase. Furthermore they found that Strobel (2008, 2009) have scaled the hydrodynamic equations by the escape flux, favoring large escape fluxes.

For H_2, Cui et al. (2008) found an escape flux from INMS measurements, which is about three times higher than the respective Jeans escape flux from Titan. However, Cui et al. (2008) found that non-thermal escape mechanisms are not required to interpret the loss of H_2 from Titan. The enhanced escape rate (relative to the Jeans value) was found using an orthogonal series expansion in a 13-moment approximation defining a non-Maxwellian velocity distribution function that includes the effects of both thermal conduction and viscosity. The effect of collisions between H_2 and N_2 below 1,600 km was found to be significant. The 13-moment model interprets the enhanced escape as a result of the accumulation of H_2 molecules on the high-energy portion of the velocity distribution function, primarily associated with the conductive heat flux.

Since atomic hydrogen is only a minor species, it diffuses through the heavier background gas towards the exobase, where it can escape. The critical value above which diffusion-limited hydrodynamic outflow of atomic hydrogen occurs, is given when the Jeans escape parameter $\Lambda(r)$ is lower than a critical value of 1.5. The escape parameter is the ratio of the potential to kinetic energy:

$$\Lambda(r) = \frac{GMm_{\mathrm{H}}}{k_B T_c r_c} = \frac{v_{\mathrm{esc}}^2}{v_{\mathrm{p}}^2}, \tag{1}$$

with G being the gravitational constant, M the mass of Titan, m_{H} the atomic hydrogen mass, r_c the exobase radius, k_B the Boltzmann constant, and T_c the exobase temperature, v_{esc} the escape velocity and v_{p} the most probable Maxwellian velocity. With an exobase temperature of $T_c = 150\,\mathrm{K}$, one obtains for atomic hydrogen $\Lambda_{\mathrm{H}} = 1.77$, which is slightly above the limit at which hydrodynamic escape occurs. The critical temperature is reached at about 178 K.

With a distance to Saturn of about 21 Saturn radii, Titan is usually located inside Saturn's magnetosphere, with a magnetopause stand-off distance of about 23 Saturn radii (Bertucci et al. 2009). Due to the lack of an own significant intrinsic magnetic field (Backes et al. 2005), Lammer et al. (1998) found that atmospheric sputtering by magnetospheric ions (protons and N^+ ions) becomes important during this time, heating the thermosphere by an amount of about 30 K. Under such conditions, they concluded that Titan's exospheric temperature may then reach or even exceed the critical temperature, at which diffusion-limited hydrodynamic escape of hydrogen atoms becomes important. However, Michael and Johnson (2005) also investigated

the energy deposition of pickup ions and found, contrary to Lammer et al. (1998), a much lower increase in the exospheric temperature of only about 4 to 7 K caused by energy deposition of N^+.

With an escape parameter of $\Lambda_H = 1.77$ one obtains a Jeans escape flux of

$$\Phi_J = \frac{1}{2\sqrt{\pi}} n_H v_p (1 + \Lambda_H) \exp(-\Lambda_H) = 1.67 \cdot 10^9 \,\mathrm{cm}^{-2}\,\mathrm{s}^{-1}, \qquad (2)$$

assuming an atomic hydrogen density of $n_H = 8 \cdot 10^4 \,\mathrm{cm}^{-3}$ at the exobase, as inferred from de La Haye et al. (2007b) as well as a most probable Maxwellian velocity of $v_p = 1,573 \,\mathrm{m\,s}^{-1}$ using an exobase temperature of $T = 150 \,\mathrm{K}$. Integrated over the whole Titan sphere this yields an escape rate of $Q_H = 1.74 \cdot 10^{27} \,\mathrm{s}^{-1}$ at the exobase or $6.95 \cdot 10^{26} \,\mathrm{s}^{-1}$, relative to the surface. However, note that since atomic hydrogen is only a minor component in Titan's upper atmosphere and exosphere, it diffuses through the heavier background gas towards the exobase, where it can escape. The atomic hydrogen escape flux is hence limited by the diffusion through the homopause. The Jeans escape velocity $v_J = \Phi_J / n_H$ for atomic hydrogen is then $v_J = 0.21 \,\mathrm{km\,s}^{-1}$.

The photo-ionization lifetime of atomic hydrogen at Saturn's distance is about $(0.58 - 1.2) \cdot 10^9 \,\mathrm{s}$ (adapted from Huebner et al. 1992). The charge-exchange of hydrogen atoms with either the solar wind or planetary-magnetospheric protons is however dominating: When the magnetopause of Saturn is compressed within the orbit of Titan, the hydrogen lifetime along the unprotected orbit will be determined by the solar wind plasma, giving a lifetime of about $(3.3 - 5.0) \cdot 10^7 \,\mathrm{s}$ (Wolfe et al. 1980). If, however, the orbit of Titan lies within the magnetosphere, the hydrogen lifetime is determined by the co-rotating plasma giving a lifetime of about $(4.4 - 7.1) \cdot 10^7 \,\mathrm{s}$ (Smyth 1981). The characteristic timescale for a hydrogen atom thermally emitted from Titan's exosphere is however much shorter. We found a characteristic timescale of $2 \cdot 10^4 \,\mathrm{s}$ for hydrogen atoms until they reach an altitude of 30,000 km above the exobase. Thus, for atomic hydrogen thermal escape is the dominant escape mechanism acting in Titan's atmosphere.

3. Instrument description

HDAC is part of the UVIS instrument aboard the Cassini orbiter. It was designed to measure the relative abundance of atomic deuterium and hydrogen from their Lyman-α emission at 121.533 nm and 121.567 nm, respectively, from Titan's and Saturn's upper atmosphere.

HDAC consists of three absorption cells separated by MgF_2-windows (see Fig. 1). The cells are filled with molecular hydrogen, oxygen and deuterium, respectively. The MgF_2-windows act as broadband filters from 115 nm up to 7.5 μm, whereas the oxygen cell should act as a narrow band filter from 115 nm to 140 nm. Unfortunately, due to a handling failure, the oxygen cell was vented prior to flight.

A 4.5 cm diameter MgF_2 lens in front of the instrument focusses the incoming radiation onto a Channel Electron Multiplier (hereafter referred to as the photodetector), with a KBr photocathode. Additionally, a baffle for suppressing scattered light is mounted in front of the instrument. HDAC has a circular field of view (FOV) of 3° in diameter. The photodetector is sensitive to radiation from about 115 nm to 240 nm. Due to the missing filter provided by the oxygen cell, HDAC is sensitive to a very broad wavelength bandpass from 115 nm up to 240 nm. Above 140 nm the intensity of the solar radiation increases rapidly with increasing wavelength, yielding a very strong background source in the measurements.

Inside the hydrogen (H) and deuterium (D) cells, tungsten filaments heat the gas and dissociate the hydrogen and deuterium molecules into atoms. These resonantly absorb the hydrogen and deuterium Lyman-α radiation passing through the cells. By switching the filaments on and off and measuring the differences in signal strength, a direct determination of the relative H- and D-Lyman-α line intensities can be made. Since the atom density in the cells depend on the filament temperature, a set of different absorption "filters" can be realized.

[Fig. 1 about here.]

Prior to the T9 flyby, HDAC was calibrated on the local interstellar medium (LISM) as well as on Jupiter. The cell optical depths determined during these inflight calibrations were lower than in preflight calibrations (Regehly 2003). The deuterium and hydrogen absorption cells of HDAC are therefore operated using a sequence of filament steps, defined by the maximum voltage level (voltage step "7") and cells off (voltage step "0") during the flyby.

At a filament step of "7" the atomic hydrogen optical depth in the H cell is τ_{HH}=0.865 (Regehly 2003), whereas the deuterium optical depth in the D cell could not be determined. Furthermore, during the cell calibration measurements of the LISM, it turned out that the D cell is contaminated

with a significant amount of atomic hydrogen. Hence, an additional atomic hydrogen optical depth of $\tau_{\rm HD}$=0.224 for the D cell must be taken into account when considering the D cell measurements with a filament step of "7". The cell temperature for both absorption cells was 300 K.

Due to the change of relative velocity of Cassini with respect to Titan during a flyby, the emitted lines are Doppler shifted with respect to the absorption in the cell. Thus, during a flyby, HDAC is able to scan through the emission line, providing a measurement of the Lyman-α line shapes.

4. Measurements

HDAC has so far only been used once because of the previously mentioned problems with the instrument. On December 26$^{\rm th}$, 2005 Cassini passed Titan during the T9 encounter. HDAC was switched on at 17:53:34h (UTC, timestep 0 in Fig. 2), having a distance to Titan's center of 25,468.9 km. Note that one timestep corresponds to an integration time of 9 s (see above). The closest approach was achieved at a distance of 12,985.0 km at 18:59:25h (UTC, timstep 419), increasing again to 23,855.9 km at the end of the observations at 19:59:33h (UTC, timestep 840). The angular diameter of Titan changed between 8° to 12° (lower panel in the figure). During the encounter, HDAC was pointing to the subsolar point on Titan's disc. After passing the terminator region after closest approach, limb scans of Titan were performed (see red lines in the lower panel of Fig. 2). During these limb measurements, Saturn was in the FOV of HDAC, contributing to the measured signal (see Fig. 3). The Doppler velocity changed from –4.70 km s^{-1} at the beginning to 4.94 km s^{-1} at the end (see Fig. 2, center panel).

[Fig. 2 about here.]

During the T9 flyby, HDAC performed 53 sequences of filament steps, with a total detector integration time of 9 s per step. The count rate at each step was measured using 72 single integrations for each step, with a duration of 0.125 s (72·0.125 s=9 s). One sequence was made of 16 voltage steps, where both cells were switched off during the first step. Afterwards the H cell was switched on for the rest of the sequence and the D cell was switched on every second step, hence the whole voltage sequence pattern reads [0777777777777777] for the H cell and [0707070707070707] for the D cell.

Figure 3 shows the measured signal during the T9 flyby. Black dots represent cell off measurements, whereas red and blue dots are measurements where only the H cell and where both cells are switched on, respectively. The intensity drops in the data arise from FOV changes (for the first two drops at timestep 310 and 450), while at the third drop (timestep 720), Cassini performed limb occultation scans, beginning with looking at the night side of Titan. Due to the few cell off patterns (H=0, D=0, every 16th step) the signal was undersampled during these FOV changes, which is clearly visible in the data shown in Fig. 3.

[Fig. 3 about here.]

At the beginning of the observations (timestep 0), HDAC measured a count rate of $1.61 \cdot 10^4\,\mathrm{cts\,s^{-1}}$ in photometer mode (both cells switched off). During the closest encounter above Titan's terminator region (timestep 413), the signal decreased to $1.41 \cdot 10^4\,\mathrm{cts\,s^{-1}}$. Afterwards, the signal increased rapidly due to Saturn being in the FOV of HDAC during the above mentioned limb measurements.

When the H cell was switched on (red dots in Fig. 3), the cell already absorbed part of the incoming radiation although the Doppler shift is very large. Since the instrument is pointing towards the sunlit side of Titan we assume that the H cell has already absorbed a tiny part of the H Lyman-α emission line, visible as a slight decrease in the signal of $1.57 \cdot 10^4\,\mathrm{cts\,s^{-1}}$ contrary to $1.61 \cdot 10^4\,\mathrm{cts\,s^{-1}}$ in photometer mode. The maximal absorption took place during the closest encounter when the Doppler shift was zero, giving a signal of $1.34 \cdot 10^4\,\mathrm{cts\,s^{-1}}$.

To determine the amount of radiation absorbed by the H cell and to remove the background provided by the missing oxygen cell, we take the difference signal of measurements taken in photometer mode (I_0) and measurements with the H cell switched on (I). Due to the undersampled signal, strong spikes occur during FOV changes. To eliminate these spikes we use the average value of cell measurements one step before and after measurements performed in photometer mode. This decreases the number of data points to 52 throughout the observation but increases the signal-to-noise ratio significantly. The final difference signal is shown in Fig. 4, giving the absorbed signal of the Lyman-α radiation emitted by Titan.

[Fig. 4 about here.]

5. Radiative transfer model description

In this section a detailed description of our radiative transfer model is given which we use to calculate the transfer of Lyman-α radiation within Titan's exosphere. The description also includes the simulation of the measurement performed by HDAC during the T9 flyby. Since HDAC is moving with time during the encounter, the radiative transfer calculations are split into two parts. The first part considers the transfer of radiation within the exosphere, whereas the second part takes into account the amount of radiation scattered into the instrument at a certain spacecraft position during the encounter. The second part is hereafter referred to as the "Data Sampling model". However in this work the entire radiative transfer model (including both parts) will be referred to as the "Monte Carlo radiative transfer model".

5.1. Radiative transfer model

In order to calculate the scattering positions within our model exosphere, we use the Monte Carlo method to solve the radiative transfer of solar Lyman-α radiation. A certain number of Lyman-α photons is traced from the point of emission (or at the beginning from the source) to the point of absorption (or the point, where the photon leaves the model without any further interaction).

We assume a spherical symmetric model exosphere with an isothermal temperature profile. In the model only resonance scattering of solar radiation on atomic hydrogen and absorption by methane is considered. The density distribution throughout the model exosphere is provided by two different models that will be described in detail in section 6. The scattering direction is assumed to be isotropic and polarization of the scattered emission is ignored. Note that the phase function for resonance scattering is not exactly isotropic, but for simplicity reasons we have chosen to neglect the small non-isotropy. We allow for pure absorption by methane molecules. Hence, photons are lost either by escape through the upper or lower model boundaries or via absorption.

The lower model boundary is set to 780 km altitude and is hence well below the exobase defined in section 2. We assume that all photons reaching the lower boundary will be absorbed by methane, as this is the altitude where CH_4 is mainly photolyzed (see section 2). The upper boundary altitude at

30,000 km has been chosen to be well above the Cassini spacecraft altitude during the T9 flyby measurements. Varying the model boundaries does not have any influence on the result. For the lower boundary almost all Lyman-α photons are already absorbed above the exobase, whereas for the upper model boundary the exosphere is already optically thin for resonance scattering.

The x-axis connects Titan's center and the Sun's position via the subsolar point on Titan's exobase. The y- and z-axes are chosen to be perpendicular, spanning a right-handed coordinate system. The orientation of both the y- and the z-axis is chosen arbitrarily.

The rotation of Titan is not considered within the radiative transfer model, since the rotational velocity of Titan is small compared to thermal velocities of atomic hydrogen. Müller-Wodarg et al. (2008) have found strong thermospheric winds reaching about $150\,\mathrm{m\,s^{-1}}$. These winds do not have any effect on the particles in the exosphere since collisions are negligible here. Furthermore, the effect of radiation pressure on the hydrogen atoms is not taken into account, since radiation pressure becomes important only above a distance to Titan of 314,709 km or $122.21\,\mathrm{R_{Titan}}$.

The incident solar radiation is assumed to enter the sunlit hemisphere of the model at the upper model boundary in a parallel beam, being perpendicular to the y-z-plane. The initial coordinates of the photons are thus chosen from a source distribution with $x > 0$. They are initially flying into the anti-sunward direction $\mathbf{k} = (-1, 0, 0)$.

Using the Monte Carlo method, single photons leaving the source in a given direction represent a large set of N real photons. Since a number fraction of N_i photons will be absorbed on the way through the exosphere within the model, the photon's weight $W = N_i/N$ is introduced, which is initially set to unity at the source.

The wavelength of the incident photons is chosen from a rectangular source distribution centered at 1215.67 Å. The solar Lyman-α profile has a width of about 1 Å and a central depression. Only this central depression is considered in this work, which is approximately constant over the wavelength range considered here. For the calculations, photons are created with a random wavelength chosen within a range of 0.0451 Å, which corresponds to five times the Doppler width, with a cell temperature of 300 K. This wavelength range covers not only the total wavelength interval over that HDAC scans within the measurements (total width of 0.0391 Å), but furthermore covers photons that are started outside the instrument bandpass and are scattered into it. A further increase of the wavelength range covered was not

found to change the result.

Knowing the direction of a photon from its starting point $\mathbf{x}_\mathrm{S}$ (either the point of insertion or the last scattering point), a given photon suffers an interaction (either scattering or absorption) after traveling a random optical depth

$$\tau_r = \ln(r_i), \tag{3}$$

where r_i is a random number, uniformly distributed in the interval (0,1).

In the model, the photons cross different density layers along their path. The path is thus a sequence of distances L_i (i=1,...,n) towards the next layer, with $L_1 = \mathbf{x}_1 - \mathbf{x}_\mathrm{S}$ and $L_\mathrm{n} = \mathbf{x}_\mathrm{n} - \mathbf{x}_{n-1}$ ($\mathbf{x}_\mathrm{n}$: model boundary). The density within a layer is assumed to be homogeneous.

In order to determine the scattering positions within the model, τ_r is compared to the accumulated optical depth τ_acc that the photon travels on its path through the atmosphere. The accumulated optical depth is given by summing up the optical depth in each layer i the photon crosses:

$$\tau_\mathrm{acc}(\lambda) = \sum_{i=1}^{n} \left[n_\mathrm{H}(i)\sigma_\mathrm{H}(\lambda) + n_{\mathrm{CH_4}}(i)\sigma_{\mathrm{CH_4}} \right] L_i, \tag{4}$$

with $n_\mathrm{H}(i)$ and $n_{\mathrm{CH_4}}(i)$ being the atomic hydrogen and methane density in each layer crossed by the photon, respectively, $\sigma_\mathrm{H}(\lambda)$ the resonance scattering cross section of atomic hydrogen, $\sigma_{\mathrm{CH_4}}$ the wavelength independent methane photodissociation cross section and s_i the length of the photon path in layer i.

For Lyman-α radiation, the methane photodissociation cross section is independent of temperature and wavelength, being $\sigma_{\mathrm{CH_4}} = 2.0 \cdot 10^{-17}$ cm^2 (Vatsa and Volpp 2001). The wavelength dependent resonance scattering cross section of atomic hydrogen however is given by

$$\sigma_\mathrm{H}(\lambda) = \frac{f_{Ly\alpha}\mu_0 e^2 \lambda_0^2}{4\sqrt{\pi} m_e \Delta\lambda_D} \exp\left[-\left(\frac{\lambda - \lambda_0}{\Delta\lambda_D} \right)^2 \right], \tag{5}$$

with e, m_e being the charge and mass of the electron, $f_{Ly\alpha}$ the oscillator strength of Lyman-α ($f_{Ly\alpha} = 0.4163$), μ_0 the permeability of free space and

$\Delta\lambda_D$ the Doppler width:

$$\Delta\lambda_D = \frac{\lambda_0}{c} v_p = \frac{\lambda_0}{c}\sqrt{\frac{2k_B T}{m_{\mathrm{H}}}}, \tag{6}$$

with k_B being the Boltzmann constant, m_{H} the mass of a hydrogen atom, T the exospheric temperature and c the speed of light. Note here, that v_p is the thermal velocity of atomic hydrogen. Equation 5 assumes that the scattering is isotropic in the atom's frame of reference.

The following cases are considered:

- If $\tau_r > \tau_{\mathrm{acc,total}}$, the photon is assumed to leave the exosphere without being scattered or absorbed. Hence, the photon is no longer considered in the calculations and a new photon is released from the source.

- If $\tau_r < \tau_{\mathrm{acc,total}}$ is fulfilled, the photon has suffered an interaction within the medium. The exact position of the event in the exosphere and the nature of the interaction is determined. At this position, the photon may either be scattered by an hydrogen atom or removed by absorption of methane. To economize computational time, photons are not absorbed in the model but are scattered further until they leave the model boundaries. Therefore, the photon's weight need to be adjusted in order to account for this. This is done by weighting each photon by the probability of absorption, which is simply given by

$$W = W_{\mathrm{old}} \cdot \exp\left(-\tau_{\mathrm{CH4}}\right), \tag{7}$$

  with W_{old} being the weight of the photon before the interaction and $\tau_{\mathrm{CH_4}}$ being the total optical depth caused by methane on the path from the last scattering point (or source) to the current position. In order to prevent photons to be scattered infinitively close to the lower model boundary, photons with a methane optical depth exceeding a value of $\tau_{\mathrm{CH_4}} > 100$ are no longer treated and a new photon is released from the source.

The new direction of the photon after scattering is assumed to be isotropic,

hence can be calculated by

$$\begin{aligned} k'_x &= \cos\phi \sin\theta \\ k'_y &= \sin\phi \sin\theta, \\ k'_z &= \cos\theta \end{aligned} \tag{8}$$

with the spherical coordinates being $\theta = \arccos(2r_i - 1)$ and $\phi = \pi(2r_j - 1)$ and r_i and r_j being two independent random variables, uniformly distributed in (0,1). The scattering angle α is given by the scalar product between the photon's incoming direction $\mathbf{k}$ and the scattering direction $\mathbf{k}'$. The scattering phase angle γ is hence $\gamma = \pi - \alpha$. $\gamma = 0°$ is equivalent to forward scattering and $\gamma = 180°$ to backward scattering.

The resonance scattering of solar radiation is a coherent process in the rest frame of the hydrogen atom. In the case of the low densities in Titan's exosphere considered here, collisions of excited atoms can be neglected. In the external frame, however, due to the movement of the atoms, the wavelength of the scattered photon is redistributed due to the Doppler effect. The wavelength of the scattered photon has thus a complex dependence on the wavelength prior to the scattering, which is formally known as "partial frequency redistribution" (Avery and House 1968).

For the calculation of the scattered photon's wavelength, the angle-dependent redistribution function from Hummer (1962) (case II in his paper) is used. Assuming a Maxwellian distribution of velocities, the redistribution function is a probability distribution of the scattered wavelength as a function of incident wavelength, and scattering phase angle γ:

$$\begin{aligned} R_{\mathrm{II}}(d, d', \gamma) &= \frac{g(\gamma)}{\sqrt{\pi}\sin\gamma} \exp\left[-\left(\frac{d - d'}{2} \csc\frac{\gamma}{2} \right)^2 \right] \\ &\times \psi\left(\alpha \sec\frac{\gamma}{2}, \frac{d + d'}{2} \sec\frac{\gamma}{2} \right) \end{aligned} \tag{9}$$

where d' and d are the initial and final wavelengths relative to the line center in units of Doppler width, $g(\gamma)$ is the scattering phase function, ψ is the Voigt function and α is the natural linewidth in Doppler units. Since isotropic scattering is assumed, $g(\gamma) = 1/(4\pi)$ applies. The final wavelength from this distribution is determined by first choosing a random wavelength d, being uniformly distributed in the wavelength range considered in this work.

Then, a second random number y_r uniformly distributed in the interval (0, $\max(R_{\rm II})$) is chosen, where $\max(R_{\rm II})$ denotes the maximum of the function. If $y_R < R_{\rm II}$ is fulfilled, the wavelength chosen before is used, otherwise a new set of values for d and y_r is generated. We note that there exists another algorithm for randomly selecting photon emission frequencies from a redistribution function by Lee (1974), which will be used in further publications in a broader context. However, for the sake of simplicity we have chosen to follow the above mentioned approach.

Using the new direction and wavelength of the emitted photon, the photon is followed until it leaves the model boundaries or is absorbed (in the case where the absorption optical depth exceeds a value of 100). Each photon is hence treated in a single way on its way through the atmosphere.

5.2. Data Sampling model

During the flyby of Cassini the altitude and position of the spacecraft changed rapidly, scanning over the whole Titan disc. In order to calculate the Lyman-α emission intensity measured by HDAC during the flyby, every scattering point within the instrument's FOV is assumed to emit a photon towards the detector. This assumption is based on the "splitting" technique described by Hammersley and Handscomb (1964): After each scattering event, the photon traveling into the new random direction $\mathbf{k}'$ is split into two, one of which travels into the direction of the detector $\mathbf{k}'_{\mathbf{D}}$, the other into the direction $\mathbf{k}'$.

Applying the splitting technique, the weight W of the photon before the scattering event needs to be split: $W = W' + W_D$, where W' and W_D are the weights of the photon flying into the new random direction and the weight of the photon flying into the direction of the detector, respectively. The other photon flying into direction $\mathbf{k}'$ hence continues its flight with a reduced weight of $W' = W - W_D$. This is of importance in cases, where a given photon undergoes two or more scattering events that lie within the FOV at a given spacecraft position. This technique is applied to every scattering point in the FOV of the instrument during the flyby. The weight of the splitted photon flying towards the detector, W_D, is given by $W_D = W \cdot \mathcal{P}_D$. Here, $\mathcal{P}_D$ is the probability that the photon will finally be detected:

$$\mathcal{P}_D(\lambda) = p_D(\lambda) \cdot \mathcal{T}_{\rm C}(\lambda_D). \tag{10}$$

Here, $p_D(\lambda)$ is the probability, that the considered photon will arrive at the

instrument, and $\mathcal{T}_{\mathrm{C}}(\lambda_D)$ is the transmission function of the cells. Since the photons are now forced to be scattered into a different direction (towards the detector), a new wavelength for the particular photon needs to be calculated, using the redistribution function (Eq. 9) and the new scattering angle. In Eq. 10, λ is this new emission wavelength, whereas λ_D is the wavelength of the photon under which it will be detected by HDAC. This is due to the movement of the detector with respect to Titan:

$$\lambda_D = \lambda + \lambda_0 \frac{v_D}{c}, \tag{11}$$

with v_D being the Doppler speed of the spacecraft.

The arrival probability $p_D(\lambda)$ includes the transmission from the scattering point to the detector $\mathcal{T}(\lambda)$, the solid angle probability of the photon to enter the detector P_Ω, and the FOV sensitivity $S_{\mathrm{FOV}}(\beta)$:

$$p_D(\lambda) = P_\Omega \cdot \mathcal{T}(\lambda) \cdot S_{\mathrm{FOV}}(\beta). \tag{12}$$

The transmission function of the cells is calculated using the cell parameters:

$$\mathcal{T}_{\mathrm{C}}(\lambda_D) = \exp\left[-\tau_{\mathrm{H}} \cdot \exp\left(\frac{\lambda_D - \lambda_0}{\Delta\lambda_{\mathrm{C}}}\right)\right], \tag{13}$$

with $\Delta\lambda_{\mathrm{C}}$ being Doppler width in the cells. When considering the measurements performed in photometer mode only, the cell transmission function is simply given by $\mathcal{T}_{\mathrm{C}}(\lambda_D) = 1$.

Finally, taking the sum of the detection probability $\mathcal{P}_D$ for all photons that are scattered within the FOV and arrive at the detector at a certain spacecraft position $\mathbf{x}_{\mathrm{Cas}}$ yield the count rate for this position:

$$n(\mathbf{x}_{\mathrm{Cas}}) = \sum_{i=0}^{j} \mathcal{P}_{D,i}. \tag{14}$$

6. Exospheric density models

Direct measurements of densities in the atmosphere of Titan are limited to altitudes below 2,000 km. Especially in the upper atmosphere only the heavier species can be measured, like nitrogen and methane. The distribution of molecular hydrogen could also be determined from mass-spectrometer data (Cui et al. 2009). However, there exists no direct measurement of the

atomic hydrogen distribution in the exosphere of Titan. The investigation of the radiative transfer in Titan's exosphere therefore requires the development of an exospheric density distribution model, so as to evaluate the altitude density profile. Above the exobase, where the hydrogen atoms no longer follow a Maxwellian distribution of velocities (since collisions are negligible), two different exospheric models are applied, briefly described in the following. Both models require the exobase density and temperature as input parameters to derive the density throughout the exosphere.

As a first approach we apply the exospheric model of Chamberlain (1963), which was developed to investigate the structure of the terrestrial exosphere. Assuming a Maxwellian distribution of velocities at the exobase and applying Liouville's theorem, the Chamberlain model implies that the velocity distribution function above the exobase is also Maxwellian, truncated to include only regions in the momentum space occupied by particles whose orbits are controlled only by gravity. Any particle in the exosphere naturally falls into one of four categories, based on orbital characteristics, i.e., ballistic, bound, escaping, and incoming hyperbolic particles. At any given point in the exosphere, each of the above types occupies an isolated region in the phase space.

Particles in bound (satellite) orbits have perigees above the exobase, and therefore have a purely exospheric origin. The existence of bound orbits depends on the balance of the rare collisions that do occur within the exosphere with the rare destructive processes, such as photo-ionization. Because in any collision-less model there is no mechanism to establish a steady-state population of bound particles, this category is excluded from the density calculations. Incoming particles on hyperbolic orbits are also excluded since they obviously require an external origin.

The particle densities are calculated by integrating over the appropriate regions of the momentum space at any height, yielding the distribution of density throughout the exosphere:

$$N(r) = n_c \exp^{-(\Lambda_c - \Lambda(r))} \zeta(\Lambda(r)), \tag{15}$$

where n_c is the density at the critical level r_c (i.e. the exobase) and Λ is the Jeans parameter given by Eq. 1.

The right hand side of Eq. 15 represents the hydrostatic equation multiplied by ζ, a partition function, which describes the orbits of the particles released at the exobase, with $\zeta = \zeta_{\rm bal} + \zeta_{\rm esc}$. Above the exobase the den-

sity departs from the barometric law only as orbits in certain directions and energy ranges become depleted.

As another approach, we use a particle model from Wurz and Lammer (2003) (furthermore referred to as the "Particle model"). It has been applied to Mercury's exosphere, to the lunar exosphere (Wurz et al. 2007), as well as to Mars's exosphere using the ASPERA-3 instrument aboard Mars Express (Galli et al. 2006). Using the Monte Carlo method, the model follows the individual trajectories of particles released from the exobase through the exosphere until the particles cross the exobase layer again or cross the upper model boundary. The initial particle velocities are chosen randomly from a Maxwellian distribution and are released into a random direction. In the model no assumptions are made for the exosphere itself, for example barometric scaling or non-barometric scaling; everything follows from the trajectory calculations. Trajectory modifications due to radiation pressure are not considered in the model, because these effects are negligible for atomic hydrogen in Titan's exosphere.

For the distribution of atomic hydrogen in the upper atmosphere from 780 km up to the exobase, data obtained from the photochemical model of Krasnopolsky (2009) are used. The distribution of atomic hydrogen above this level up to the upper model boundary is calculated by the afore mentioned models. Note that the choice of the hydrogen distribution below the exobase has only a minor effect on the calculation result, since almost all photons are absorbed by methane already above the exobase. The methane profile used in the radiative transfer model is taken from de La Haye et al. (2008) in the altitude range from 780 km to 2,000 km. Above, the methane profile has been extrapolated again by using the Particle model (see Fig. 5).

Using both models with a fixed exobase temperature of $T = 150\,\mathrm{K}$ and an exobase density of $n_\mathrm{H} = 1 \cdot 10^4\,\mathrm{cm}^{-3}$ (as shown in Fig. 5) yields the main difference in the profiles both models produce. The Chamberlain model yields higher densities in the upper exosphere; the density decreases much faster with altitude using the Particle model. At the exobase the Chamberlain model shows a strong change of the density gradient: below the exobase the density decreases strongly with increasing altitude, and above the decrease is much slower. This is also observed when using the Particle model, however, the transition is much smoother. The different density gradients below and above the exobase occur since below the exobase hydrostatic equilibrium is maintained, whereas above particles are ballistically flowing away from Titan.

[Fig. 5 about here.]

7. Fit to measured data

Before fitting the modeled data to the observations during the T9 flyby, we performed a parameter variation to infer the response of the signal when taking the two different atomic hydrogen profiles provided by the density distribution models. Furthermore, we varied the exobase density as well as the exospheric temperature, which are both input parameters for the density models. Afterwards we compared the difference signal of calculations performed with and without considering the absorption of the H cell with the difference signal measured during the T9 flyby. For each density profile, we performed a least squares fit, to determine the best fitting exobase density and temperature.

We were able to fit both density profiles (see Fig. 6), however, with a large difference in exobase densities. With a Chamberlain model profile we found a best fitting exobase density of $n_{\mathrm{H}} = (1.5 \pm 0.5) \cdot 10^4\,\mathrm{cm}^{-3}$, using an exospheric temperature of $T_{\mathrm{H}} = (150 \pm 25)\,\mathrm{K}$. However, when using the profile provided by the Particle model, we found that a best fitting exobase density of $n_{\mathrm{H}} = (7 \pm 1) \cdot 10^4\,\mathrm{cm}^{-3}$ together with an exospheric temperature of $T_{\mathrm{H}} = (175 \pm 25)\,\mathrm{K}$ is required to fit the data, which can be seen from Fig. 7. This difference in exobase densities results from the different density gradients in the model profiles. The Chamberlain profile has a much higher density in the upper part of the exosphere, allowing more photons to be scattered.

[Fig. 6 about here.]

The reason for the difference in the required exobase densities on the one hand and the ability to fit the profiles provided by both exospheric model on the other hand is the altitude to which HDAC is sensitive to. During the closest approach, Cassini had an altitude of 10,410 km. At this point, the optical depth of the atmosphere at Lyman-α as seen from the instrument becomes unity at an altitude of about 3,500 km (see thick lines in Fig. 7). Hence, HDAC is sensitive to altitudes well above the exobase altitude. Above 3,500 km, the profiles provided by both exospheric models have comparable densities, as can be seen in Fig. 8,where the density profiles above 3,500 km

are shown together with the uncertainty of the fit. To determine, which exospheric model better describes Titan's hydrogen exosphere, additional measurements with a lower noise level are required at lower flyby altitudes.

[Fig. 7 about here.]

[Fig. 8 about here.]

Using the density profile computed by the Particle model, the resulting exobase atomic hydrogen densities are in perfect agreement with the value inferred by (Krasnopolsky 2009). However, when using the density distribution calculated by the Chamberlain model, the best fitting exobase value is lower than the Voyager measurement as well as the exobase density inferred from current photochemical models (see Table 1).

During the Voyager 1980 Titan flyby, the solar Lyman-α irradiance was about 1.5 times higher than during the T9 encounter. During higher solar activity more hydrogen will be produced, hence the atomic hydrogen exobase density will be higher. Unfortunately there exists no publication describing the data retrieval from the Voyager data for atomic hydrogen. When assuming that also a Chamberlain profile has been used to fit the data, our atomic hydrogen exobase density determined using a Chamberlain profile is consistent with the Voyager measurements: With an exobase density of $1.5 \cdot 10^4\,\mathrm{cm}^{-3}$, we get a factor of 2.6 lower exobase density than Broadfoot et al. (1981), being $4 \cdot 10^4\,\mathrm{cm}^{-3}$.

The best fitting exospheric temperatures are within the range of temperatures found by other Cassini measurements. INMS measurements by de La Haye et al. (2007b) indicated a temperature in the range of 147 K to 228 K, when fitting a Maxwellian velocity distribution to the data, whereas measurements by the UVIS instrument inferred an exospheric temperature of 150 K to 250 K (D. Shemansky, priv. com.).

The best fitting temperature of 175 K required by using the Particle model for the density distribution is thus very close to the critical temperature, above which diffusion-limited hydrodynamic outflow of atomic hydrogen would occur. Nevertheless, the uncertainty in the determination as well as the assumption of an isothermal exosphere does not allow a judgement, which conditions applied for Titan at the time of the flyby.

[Table 1 about here.]

8. Results & Conclusions

This work provides for the first time information on the distribution of atomic hydrogen in the upper exosphere of Titan. Based on HDAC measurements performed during the Cassini T9 encounter, we performed Monte Carlo radiative transfer calculations to simulate the measurements. HDAC was originally designed to directly determine the D/H ratio of the atmospheres of Saturn and Titan by measuring the relative abundance of atomic deuterium and hydrogen from their Lyman-α emission at 121.533 nm and 121.567 nm, respectively.

Applying two different exospheric density models, we found that due to a strong noise pattern in the data recorded by HDAC and the high flyby altitude, the two models could be fitted to the measurement. However, both exospheric models have their main differences in the lower exosphere.

We first applied the widely-used Chamberlain model and found a best fitting exobase atomic hydrogen densities of $n_{\mathrm{H}} = (1.5 \pm 0.5) \cdot 10^4\,\mathrm{cm}^{-3}$, which is a factor of about 2.6 lower than the so far only value inferred from measurements by Voyager 1. Furthermore, the density is up to a factor of about 4.6 lower than current values from photochemical models. We therefore applied a second model, which does not rely on the truncation of the Maxwell-Boltzmann distribution in a collisionless exosphere. This model rather calculates the trajectories of particles released from the exobase to infer the density profile, without making assumptions about the exosphere. With this model, we found a best fitting exobase density of $n_{\mathrm{H}} = (7 \pm 1) \cdot 10^4\,\mathrm{cm}^{-3}$, which is a factor of 1.75 times higher than the Voyager measurement. However, current photochemical models also indicate higher exobase densities. Our best fitting density is in perfect agreement with the value inferred from latest photochemical modeling performed by Krasnopolsky (2009).

Furthermore, we were able to determine the temperature of Titan's exosphere, assuming a temperature isoprofile. With a temperature of $T_H = (175 \pm 25)\,\mathrm{K}$, that we obtain when applying the Particle model, the flux of atomic hydrogen is close to diffusion-limited hydrodynamic escape conditions. This temperature is comparable to other measurements by Cassini.

Based on the results of this work, HDAC will be used again during two flybys in 2010. Having identified the undersampling as the main source of uncertainties in the measurements of the T_9 encounter, a different measurement strategy will be used during these future flybys. Thus, these flybys will provide a more accurate determination of the exospheric atomic hydrogen

densities and temperatures.

Acknowledgements

We thank two anonymous referees for their helpful comments. We would like to thank Philip von Paris, Beate Patzer, Daniel Kitzmann and Joachim Stock for very helpful discussions. We thank Andreas Luber for helping us with the NASA SPICE system, and Audrey Schauffelberger for helpful information on the Particle model. We are grateful to the UVIS team, for providing us the HDAC data.

References

Avery, L.W., House, L.L., 1968. An Investigation of Resonance-Line Scattering by the Monte Carlo Technique. Astrophysical Journal 152.

Backes, H., Neubauer, F.M., Dougherty, M.K., Achilleos, N., André, N., Arridge, C.S., Bertucci, C., Jones, G.H., Khurana, K.K., Russell, C.T., Wennmacher, A., 2005. Titan's Magnetic Field Signature During the First Cassini Encounter. Science 308, 992–995.

Bertucci, C., Sinclair, B., Achilleos, N., Hunt, P., Dougherty, M.K., Arridge, C.S., 2009. The variability of Titan's magnetic environment. Planetary & Space Sciences 57, 1813–1820.

Broadfoot, A.L., Sandel, B.R., Shemansky, D.E., Holberg, J.B., Smith, G.R., Strobel, D.F., McConnell, J.C., Kumar, S., Hunten, D.M., Atreya, S.K., Donahue, T.M., Moos, H.W., Bertaux, J.L., Blamont, J.E., Pomphrey, R.B., Linick, S., 1981. Extreme ultraviolet observations from Voyager 1 encounter with Saturn. Science 212, 206–211.

Chamberlain, J.W., 1963. Planetary coronae and atmospheric evaporation. Planetary and Space Science 11, 901.

Cui, J., Yelle, R.V., Volk, K., 2008. Distribution and escape of molecular hydrogen in Titan's thermosphere and exosphere. Journal of Geophysical Research (Planets) 113, E10004.

Cui, J., Yelle, R.V., Vuitton, V., Waite, J.H., Kasprzak, W.T., Gell, D.A., Niemann, H.B., Müller-Wodarg, I.C.F., Borggren, N., Fletcher, G.G., Patrick, E.L., Raaen, E., Magee, B.A., 2009. Analysis of Titan's neutral upper atmosphere from Cassini Ion Neutral Mass Spectrometer measurements. Icarus 200, 581–615.

de La Haye, V., Waite, J.H., Cravens, T.E., Nagy, A.F., Johnson, R.E., Lebonnois, S., Robertson, I.P., 2007a. Titan's corona: The contribution of exothermic chemistry. Icarus 191, 236–250.

de La Haye, V., Waite, J.H., Cravens, T.E., Robertson, I.P., Lebonnois, S., 2008. Coupled ion and neutral rotating model of Titan's upper atmosphere. Icarus 197, 110–136.

de La Haye, V., Waite, J.H., Johnson, R.E., Yelle, R.V., Cravens, T.E., Luhmann, J.G., Kasprzak, W.T., Gell, D.A., Magee, B., Leblanc, F., Michael, M., Jurac, S., Robertson, I.P., 2007b. Cassini Ion and Neutral Mass Spectrometer data in Titan's upper atmosphere and exosphere: Observation of a suprathermal corona. Journal of Geophysical Research (Space Physics) 112, E7309.

Esposito, L.W., Barth, C.A., Colwell, J.E., Lawrence, G.M., McClintock, W.E., Stewart, A.I.F., Keller, H.U., Korth, A., Lauche, H., Festou, M.C., Lane, A.L., Hansen, C.J., Maki, J.N., West, R.A., Jahn, H., Reulke, R., Warlich, K., Shemansky, D.E., Yung, Y.L., 2004. The Cassini Ultraviolet Imaging Spectrograph Investigation. Space Science Reviews 115, 299–361.

Fulchignoni, M., Ferri, F., Angrilli, F., Ball, A.J., Bar-Nun, A., Barucci, M.A., Bettanini, C., Bianchini, G., Borucki, W., Colombatti, G., Coradini, M., Coustenis, A., Debei, S., Falkner, P., Fanti, G., Flamini, E., Gaborit, V., Grard, R., Hamelin, M., Harri, A.M., Hathi, B., Jernej, I., Leese, M.R., Lehto, A., Lion Stoppato, P.F., López-Moreno, J.J., Mäkinen, T., McDonnell, J.A.M., McKay, C.P., Molina-Cuberos, G., Neubauer, F.M., Pirronello, V., Rodrigo, R., Saggin, B., Schwingenschuh, K., Seiff, A., Simões, F., Svedhem, H., Tokano, T., Towner, M.C., Trautner, R., Withers, P., Zarnecki, J.C., 2005. In situ measurements of the physical characteristics of Titan's environment. Nature 438, 785–791.

Galli, A., Wurz, P., Lammer, H., Lichtenegger, H.I.M., Lundin, R., Barabash, S., Grigoriev, A., Holmström, M., Gunell, H., 2006. The Hydrogen Exospheric Density Profile Measured with ASPERA-3/NPD. Space Science Reviews 126, 447–467.

Garnier, P., Dandouras, I., Toublanc, D., Brandt, P.C., Roelof, E.C., Mitchell, D.G., Krimigis, S.M., Krupp, N., Hamilton, D.C., Waite, H., 2007. The exosphere of Titan and its interaction with the kronian magnetosphere: MIMI observations and modeling. Planetary and Space Science 55, 165–173.

Hammersley, J.M., Handscomb, D.C., 1964. Monte Carlo Methods. Methuen and Co., London.

Huebner, W.F., Keady, J.J., Lyon, S.P., 1992. Solar photo rates for planetary atmospheres and atmospheric pollutants. Astrophysics & Space Science 195, 1–289.

Hummer, D.G., 1962. Non-coherent scattering: I. The redistribution function with Doppler broadening. Monthly Notices of the Royal Astronomical Society 125, 21–37.

Krasnopolsky, V.A., 2009. A photochemical model of Titan's atmosphere and ionosphere. Icarus 201, 226–256.

Lammer, H., Stumptner, W., Bauer, S.J., 1998. Dynamic escape of H from Titan as consequence of sputtering induced heating. Planetary & Space Sciences 46, 1207–1213.

Lee, J., 1974. Monte Carlo Simulation of Emission Frequencies from Partial Frequency Redistribution Functions. Astrophysical Journal 192, 465–474.

Magee, B.A., Waite, J.H., Mandt, K.E., Westlake, J., Bell, J., Gell, D.A., 2009. INMS-derived composition of Titan's upper atmosphere: Analysis methods and model comparison. Planetary & Space Sciences 57, 1895–1916.

Michael, M., Johnson, R.E., 2005. Energy deposition of pickup ions and heating of Titan's atmosphere. Planetary & Space Sciences 53, 1510–1514.

Müller-Wodarg, I.C.F., Yelle, R.V., Cui, J., Waite, J.H., 2008. Horizontal structures and dynamics of Titan's thermosphere. Journal of Geophysical Research (Planets) 113, E10005.

Regehly, M., 2003. Characterization and Verification of the Hydrogen Deuterium Absorption Cell. Master's thesis. Humboldt University, Berlin.

Smyth, W.H., 1981. Titan's hydrogen torus. Astrophysical Journal 246, 344–353.

Strobel, D.F., 1983. Photochemistry of the Reducing Atmospheres of Jupiter, Saturn and Titan. International Reviews in Physical Chemistry 3, 145–176.

Strobel, D.F., 2008. Titan's hydrodynamically escaping atmosphere. Icarus 193, 588–594.

Strobel, D.F., 2009. Titan's hydrodynamically escaping atmosphere: Escape rates and the structure of the exobase region. Icarus 202, 632–641.

Toublanc, D., Parisot, J.P., Brillet, J., Gautier, D., Raulin, F., McKay, C.P., 1995. Photochemical modeling of Titan's atmosphere. Icarus 113, 2–26.

Tucker, O.J., Johnson, R.E., 2009. Thermally driven atmospheric escape: Monte Carlo simulations for Titan's atmosphere. Planetary & Space Sciences 57, 1889–1894.

Vatsa, R.K., Volpp, H.R., 2001. Absorption Cross Sections for Some Atmospherically Important Molecules at the H Atom Lyman-a Wavelength (121.567 nm) . Chemical Physical Letters 340, 289–295.

Vervack, R.J., Sandel, B.R., Strobel, D.F., 2004. New perspectives on Titan's upper atmosphere from a reanalysis of the Voyager 1 UVS solar occultations. Icarus 170, 91–112.

Vuitton, V., Yelle, R.V., Cui, J., 2008. Formation and distribution of benzene on Titan. Journal of Geophysical Research (Planets) 113, E5007.

Waite, J.H., Lewis, W.S., Kasprzak, W.T., Anicich, V.G., Block, B.P., Cravens, T.E., Fletcher, G.G., Ip, W.H., Luhmann, J.G., McNutt, R.L., Niemann, H.B., Parejko, J.K., Richards, J.E., Thorpe, R.L., Walter, E.M., Yelle, R.V., 2004. The Cassini Ion and Neutral Mass Spectrometer (INMS) Investigation. Space Science Reviews 114, 113–231.

Wang, J., Liu, K., Min, Z., Su, H., Bersohn, R., Preses, J., Larese, J.Z., 2000. Vacuum ultraviolet photochemistry of CH4 and isotopomers. II. Product channel fields and absorption spectra. Journal of Chemical Physics 113, 4146–4152.

Wilson, E.H., Atreya, S.K., 2004. Current state of modeling the photochemistry of Titan's mutually dependent atmosphere and ionosphere. Journal of Geophysical Research (Planets) 109, 6002.

Wolfe, J.H., Mihalov, J.D., Collard, H.R., McKibbin, D.D., Frank, L.A., Intriligator, D.S., 1980. Preliminary results on the plasma environment of Saturn from the Pioneer 11 plasma analyzer experiment. Science 207, 403–407.

Wurz, P., Lammer, H., 2003. Monte-Carlo simulation of Mercury's exosphere. Icarus 164, 1–13.

Wurz, P., Rohner, U., Whitby, J.A., Kolb, C., Lammer, H., Dobnikar, P., Martín-Fernández, J.A., 2007. The lunar exosphere: The sputtering contribution. Icarus 191, 486–496.

Yelle, R.V., Cui, J., Müller-Wodarg, I.C.F., 2008. Methane escape from Titan's atmosphere. Journal of Geophysical Research (Planets) 113, E10003.

Tables

Table 1: Overview of atomic hydrogen exobase densities found in the literature

Exobase density [cm^{-3}]	Method	Reference
$(1.5 \pm 0.5) \cdot 10^4$	Chamberlain model	This work
$4.0 \cdot 10^4$	Measurement	Broadfoot et al. (1981)
$4.6 \cdot 10^4$	Model	Garnier et al. (2007)
$7.0 \cdot 10^4$	Model	Krasnopolsky (2009)
$(7.0 \pm 1.0) \cdot 10^4$	Particle model	This work
$8.0 \cdot 10^4$	Model	de La Haye et al. (2007b)

Figure captions

- Fig. 1: Detailed overview of HDAC, which is part of the UVIS instrumental package aboard the Cassini orbiter.

- Fig. 2: Orbital parameters during the T9 encounter. Top panel showing the distance to Titan, the center panel showing Doppler velocity, and the bottom panel diameter of Titan's disc and the size and position of the FOV projected on Titan's disc (red lines). Here, the center red line indicates the footpoint of the FOV, whereas the adjacent lines correspond to the FOV boundaries.

- Fig. 3: HDAC measurement during T9 encounter with Titan. Black dots are cell OFF measurements, whereas red and blue dots are measurements, where either the H cell or both cells were switched on, respectively. The vertical dotted line indicates the time of closest approach of Cassini.

- Fig. 4: Difference signal of measurements performed in photometer mode (I_0) and when the H cell was switched on (I).

- Fig. 5: Density distribution of atomic hydrogen, as calculated by the Particle model (solid line) and compared to the Chamberlain model (dotted line). The atomic hydrogen exobase density chosen for both models was $n_{\mathrm{H}} = 1 \cdot 10^4\,\mathrm{cm}^{-3}$, whereas the exobase temperature chosen was $T = 150\,\mathrm{K}$. Additionally the methane density distribution is shown (long dashed line). The shaded area indicates the altitude range of HDAC during the T9 flyby.

- Fig. 6: Best fit to measured data. Thick black diamonds show the measured difference signal during T9. Small red and blue diamonds show the best model fit, using the Chamberlain model profile and the Particle model profile, respectively.

- Fig. 7: Best fitting atomic hydrogen profile using the Particle model (solid line) as compared to the best fitting profile using the Chamberlain model (dashed line). In the figure, thick lines indicate at which altitudes the atmosphere becomes opaque at Lyman-α, as seen from HDAC during the encounter. The shaded area indicates the altitude range of HDAC during the T9 flyby.

- Fig. 8: Best fitting density profile of the Particle model (black solid line) as well as of the Chamberlain distribution (red solid line) in the altitude range, HDAC is sensitive for. The error bar of these fits is indicated by long-dashed lines.

Figures

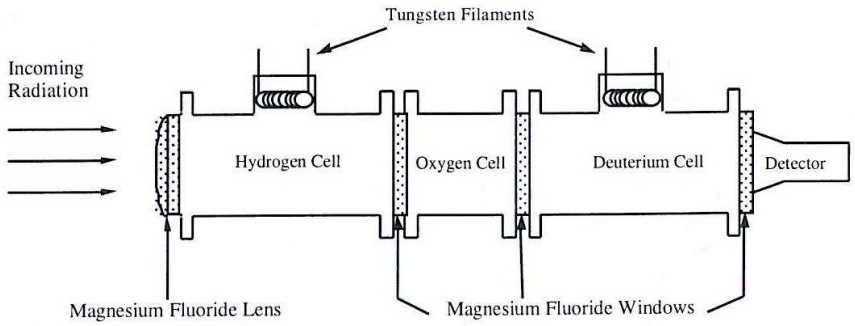

Figure 1:

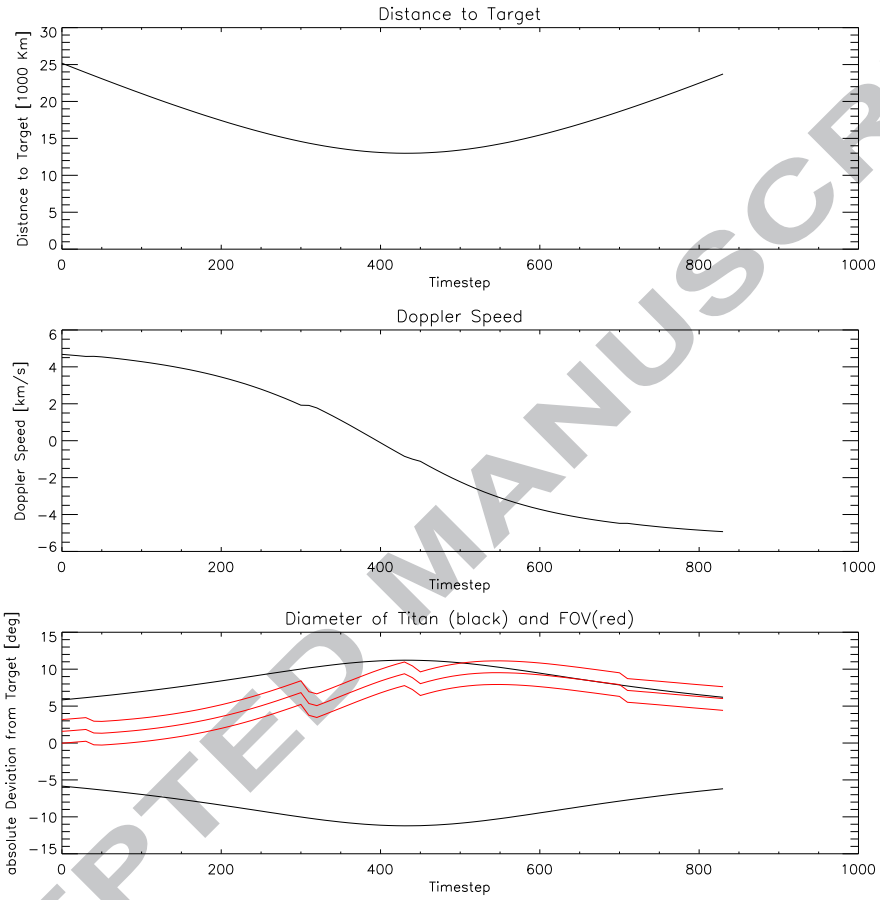

Figure 2:

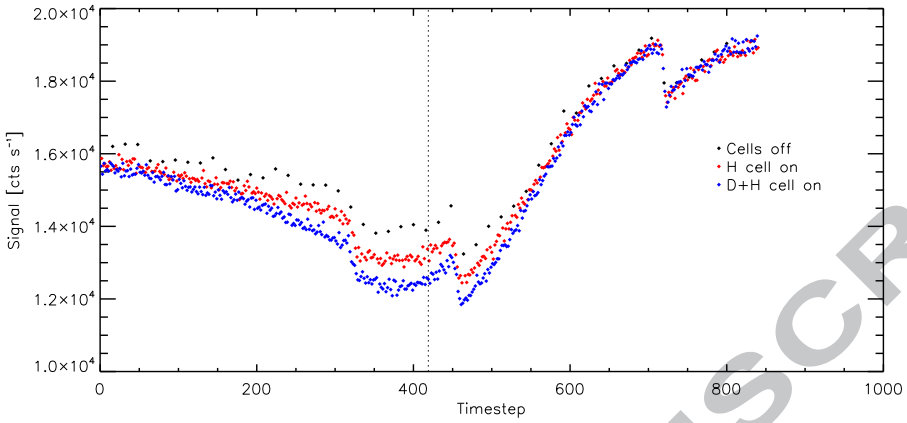

Figure 3:

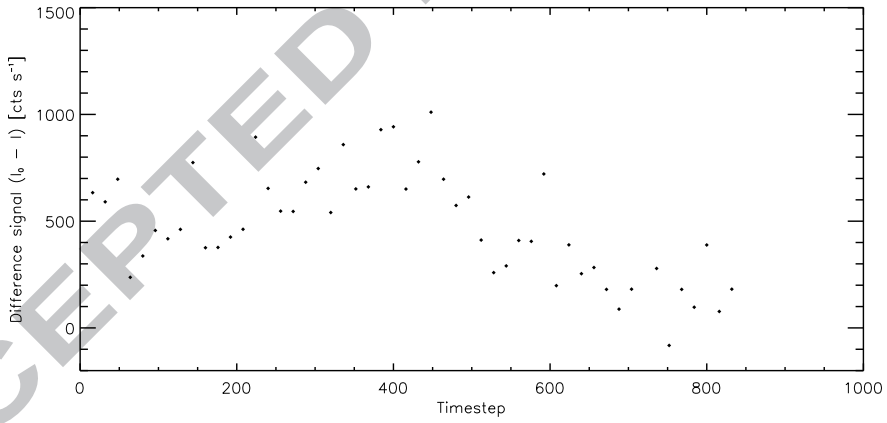

Figure 4:

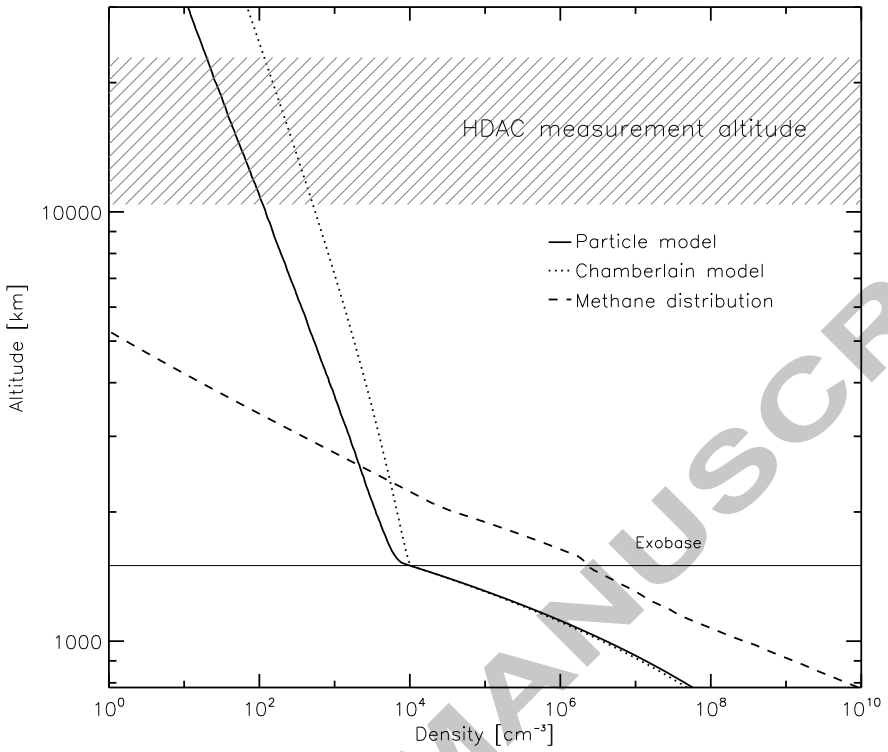

Figure 5:

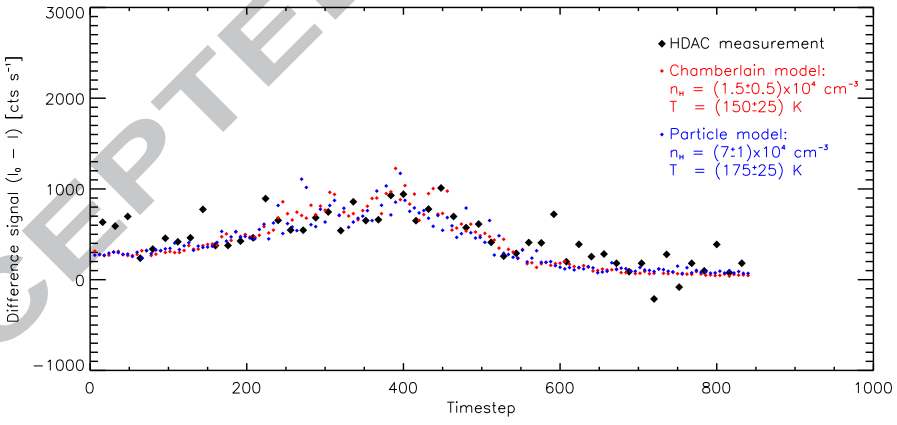

Figure 6:

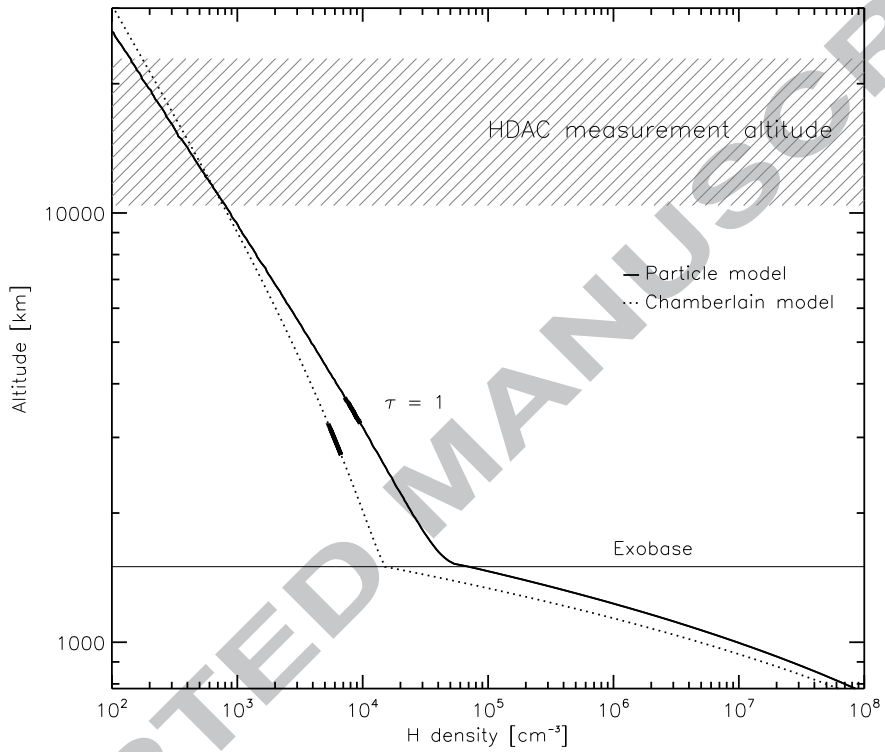

Figure 7:

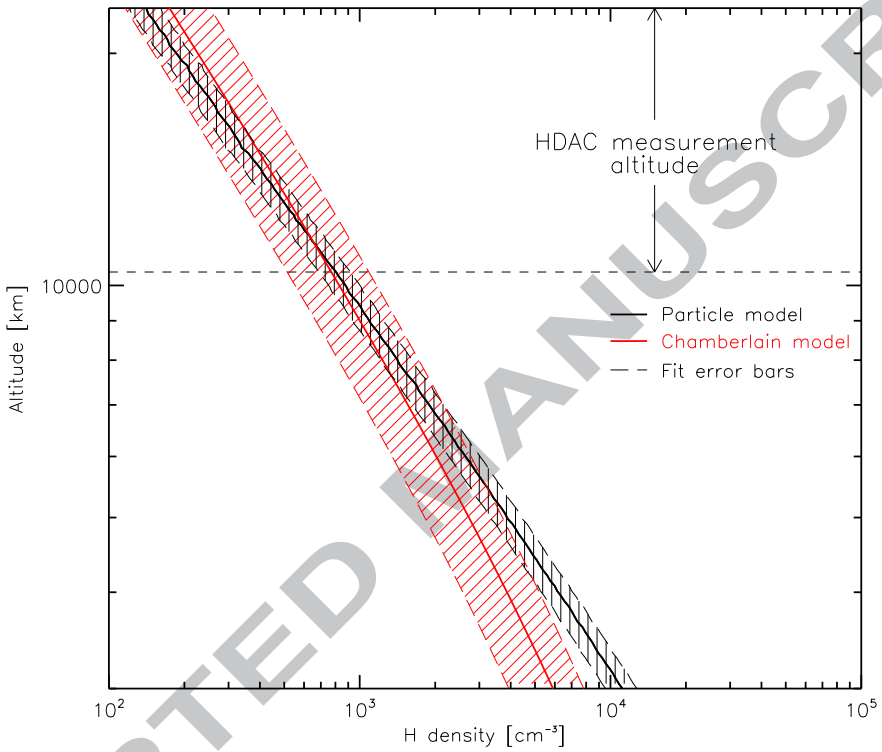

Figure 8: